Chapter 12

HYDRODYNAMIC CONSTITUTIVE RELATIONS FOR INTERFACIAL TRANSFER

In analyzing the interfacial force and relative motion between phases, consider first, the momentum equation for each phase. Under the assumption that both the average pressure and stress in the bulk fluid and at the interface are approximately the same, the k-phase momentum equation is given by

$$\alpha_k \overline{\overline{\rho}}_k \left(\frac{\partial \widehat{\boldsymbol{v}}_k}{\partial t} + \widehat{\boldsymbol{v}}_k \cdot \nabla \widehat{\boldsymbol{v}}_k \right) = -\alpha_k \nabla \overline{\overline{p}}_k + \nabla \cdot \left[\alpha_k \left(\overline{\overline{\boldsymbol{\tau}}}_k + \boldsymbol{\tau}_k^T \right) \right] + \alpha_k \overline{\overline{\rho}}_k \boldsymbol{g} + \boldsymbol{M}_{ik} + \left(\widehat{\boldsymbol{v}}_{ki} - \widehat{\boldsymbol{v}}_k \right) \Gamma_k - \nabla \alpha_k \cdot \overline{\overline{\boldsymbol{\tau}}}_{ki} \tag{12-1}$$

where $\overline{\overline{\boldsymbol{\tau}}}_k$, $\boldsymbol{\tau}_k^T$, $\overline{\overline{\boldsymbol{\tau}}}_{ki}$, and $\boldsymbol{M}_{ik}$ are the average viscous stress tensor, the average turbulent stress tensor, the interfacial shear stress, and the generalized interfacial drag force. The conservation of the mixture momentum requires

$$\sum_k \boldsymbol{M}_{ik} = 0 \tag{12-2}$$

which is the modified form of the average momentum-jump condition. Constitutive equations of the average turbulent stress tensor and the generalized interfacial drag force are required to analyze two-phase flows using the two-fluid model.

In a macroscopic two-phase flow analysis such as a one-dimensional two-phase flow analysis, the average turbulent stress term may be neglected except the wall shear contributions, whereas in a microscopic bubbly flow analysis, turbulence models such as mixing length model and k-ε model has

been attempted to estimate the average turbulent stress term. However, due to the complexity of the two-phase flow turbulence, an accurate method to predict the turbulence in two-phase flow has not been established well.

In the two-fluid momentum equation, the most important term to be modeled by a constitutive relation is the generalized drag force $\boldsymbol{M}_{id}$ which specifies the interfacial surface forces. The simplest way to model this force is to formulate as the linear combination of various known interfacial forces as

$$\begin{aligned}\boldsymbol{M}_{id} &= \frac{\alpha_d}{B_d}\left(\boldsymbol{F}_d^D + \boldsymbol{F}_d^V + \boldsymbol{F}_d^B + \boldsymbol{F}_d^L + \boldsymbol{F}_d^W + \boldsymbol{F}_d^T\right) \\ &= \boldsymbol{M}_d^D + \boldsymbol{M}_d^V + \boldsymbol{M}_d^B + \boldsymbol{M}_d^L + \boldsymbol{M}_d^W + \boldsymbol{M}_d^T\end{aligned} \tag{12-3}$$

where B_d, $\boldsymbol{F}^D$, $\boldsymbol{F}^V$, $\boldsymbol{F}^B$, $\boldsymbol{F}^L$, $\boldsymbol{F}^W$, and $\boldsymbol{F}^T$ are the volume of a typical particle, the standard drag force, the virtual mass force, the Basset force, the lift force, the wall lift force and turbulent dispersion force for a typical single particle, respectively.

The significance of the various terms in the equation is as follows. The term on the left-hand side is the combined generalized interfacial drag force acting on the dispersed phase. The first term on the right-hand side is the skin and form drag under the steady-state condition. The second term is the force required to accelerate the apparent mass of the surrounding phase when the relative velocity changes. The third term, known as the Basset force, is the effect of the acceleration on the viscous drag and the boundary-layer development. The fourth term is the lift force normal to the relative velocity due to rotation of fluid. The fifth term is the wall lift force due to the velocity distribution change around particles near a wall. The last term is the turbulent dispersion force due to the concentration gradient. In a macroscopic two-phase flow analysis such as a one-dimensional two-phase flow analysis, forces except the standard drag force and the virtual mass force are not taken into account, whereas additional forces such as the lift force and the turbulent dispersion force are also considered in a microscopic analysis for three-dimensional flow.

In the present chapter, the constitutive equations for the interfacial transfer and the interfacial fluid mechanics of multiphase flows are discussed in detail following Ishii and Zuber (1979), Ishii and Chawla (1979) and Ishii and Mishima (1984). In the following discussion, symbols designating the time-average are omitted for simplicity except in the Section 1.4 of Chapter 12.

1.1 Transient forces in multiparticle system

The forms of the two transient terms are not firmly established. Because of their importance under transient conditions and for numerical-stability problems, further research in this area is required.

The Basset force is given by

$$\boldsymbol{F}_d^B = 6r_d^2\sqrt{\pi\rho_c\mu_m}\int_t \frac{D_d}{D\xi}(\boldsymbol{v}_c - \boldsymbol{v}_d)\frac{d\xi}{\sqrt{t-\xi}} \tag{12-4}$$

where μ_m is the mixture viscosity. This term represents the additional drag due to the development of boundary layer or viscous flow during a transient acceleration of particles. The derivative D_k/Dt is the convective derivative relative to velocity $\boldsymbol{v}_k$. The subscripts c and d stand for continuous phase and dispersed phase, respectively. The detailed expression for mixture viscosity is given in the Section 1.2 of Chapter 12. Due to its complicated time-integral form, the Basset force is not considered in a practical two-phase flow analysis. Some evaluation of this term for a higher Reynolds number is given by Clift et al. (1978).

Zuber (1964a) studied the effect of the concentration on the virtual mass force and obtained.

$$\frac{\alpha_d \boldsymbol{F}_d^V}{B_d} = -\frac{1}{2}\alpha_d\frac{1+2\alpha_d}{1-\alpha_d}\rho_c\frac{D_d}{Dt}(\boldsymbol{v}_d - \boldsymbol{v}_c). \tag{12-5}$$

Lahey et al. (1978) studied a necessary condition for the constitutive equation for the virtual mass term. From the requirement of the frame-indifference of the constitutive equation, they determined that the virtual mass force $\boldsymbol{F}_d^V$ should satisfy

$$\boldsymbol{F}_d^V \propto \left[\frac{D_d\boldsymbol{v}_d}{Dt} - \frac{D_c\boldsymbol{v}_c}{Dt} + (1-\lambda)\boldsymbol{v}_r\cdot\nabla\boldsymbol{v}_r\right]. \tag{12-6}$$

In view of Zuber's study (1964a) on the effect of concentration and the above frame-indifference condition, a new form for $\boldsymbol{F}_d^V$ is proposed here. Due to the acceleration of the particles relative to the fluid, the acceleration drag arises. This should be proportional to the induced mass $\rho_c\boldsymbol{B}_d^*$ and the frame-indifferent relative-acceleration vector. Hence,

$$\boldsymbol{F}_d^V = -\rho_c B_d^* \left[\frac{D_d \boldsymbol{v}_d}{Dt} - \frac{D_c \boldsymbol{v}_c}{Dt} + (1-\lambda)\boldsymbol{v}_r \cdot \nabla \boldsymbol{v}_r \right]. \tag{12-7}$$

The value of induced mass $\rho_c \boldsymbol{B}_d^*$ for a single particle in an infinite medium can be obtained from potential theory. Hence, the limiting value of $\boldsymbol{F}_d^V$ at $\alpha_d \to 0$ for a spherical particle is

$$\lim_{\alpha_d \to 0} \boldsymbol{F}_d^V = -\frac{1}{2} \rho_c B_d \frac{D_d (\boldsymbol{v}_d - \boldsymbol{v}_c)}{Dt}. \tag{12-8}$$

From this limit, it can be shown that

$$\lim_{\alpha_d \to 0} B_d^* = \frac{1}{2} B_d \tag{12-9}$$

and

$$\lim_{\alpha_d \to 0} \lambda = 2. \tag{12-10}$$

If λ is constant in Eq.(12-7), the value of λ should be 2.

The effect of the concentration on $\boldsymbol{B}_d^*$ can be taken into account by the method used by Zuber (1964a). Thus, from the solution for the induced mass for a sphere moving within an outer sphere, $\boldsymbol{B}_d^*$, may be approximated by

$$B_d^* \doteq \frac{1}{2} B_d \frac{1+2\alpha_d}{1-\alpha_d} \tag{12-11}$$

where α_d is the volumetric fraction of the dispersed phase. Under the assumption of λ=constant, the constitutive equation for the virtual mass force is obtained from Eqs.(12-7) and (12-11) as (Ishii and Mishima, 1984)

$$\frac{\alpha_d \boldsymbol{F}_d^V}{B_d} = -\frac{1}{2} \alpha_d \frac{1+2\alpha_d}{1-\alpha_d} \rho_c \left(\frac{D_d \boldsymbol{v}_r}{Dt} - \boldsymbol{v}_r \cdot \nabla \boldsymbol{v}_c \right). \tag{12-12}$$

The above equation indicates that the virtual mass force $\boldsymbol{F}_d^V$ per particle increases considerably with increasing particle concentration. This relation implies that the effect of concentration on dynamic coupling can be scaled by a factor of $(1+2\alpha_d)/(1-\alpha_d)$. Mokeyev (1977) used an

electrohydrodynamic analog method to determine the velocity potential through an electric field potential and obtained an empirical function $B_d^*/B_d = 0.5 + 2.1\alpha_d$. The theoretical result of Eq.(12-12) compared favorably with this correlation.

A correlation for the virtual mass force in a slug flow can be developed from a simple potential flow analysis using a Bernoulli equation. First a cylindrical bubble of length L_b with diameter D_b in a tube of diameter D is considered, see Fig.12-1(a). Then the void fraction in a slug bubble section is given by

$$\alpha_b = \frac{D_b^2}{D^2} \tag{12-13}$$

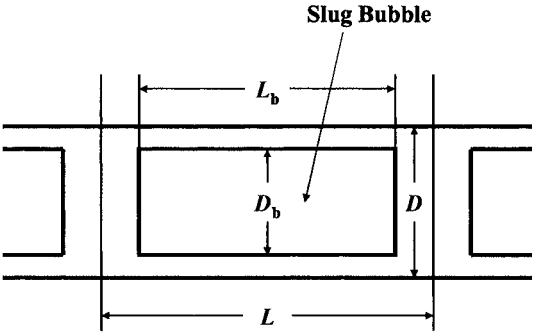

(a) Cylindrical Bubble

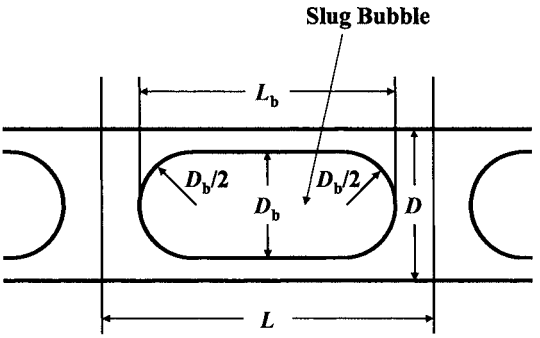

(b) Spherical-edged Cylindrical Bubble

Figure 12-1. Slug-flow model for virtual-mass-force analysis (Ishii and Mishima, 1984)

and the average overall void fraction α_d by

$$\alpha_d = \frac{L_b}{L}\alpha_b \tag{12-14}$$

where L is the pitch. Now let the continuous phase accelerate with respect to a bubble. This will generate a pressure force acting on a bubble due to the acceleration along the film section. From a simple one-dimensional analysis, this force can be found as

$$\boldsymbol{F}_d^V = -\frac{\pi}{4} D_b^2 L_b \frac{\rho_c}{1-\alpha_b}\frac{\partial \boldsymbol{v}_r}{\partial t}. \tag{12-15}$$

However, the volume of a bubble is given by $B_d = \left(\pi/4\right) D_b^2 L_b$, thus the virtual mass force per unit volume becomes

$$\frac{\alpha_d \boldsymbol{F}_d^V}{B_d} = -\alpha_d \frac{\rho_c}{1-\alpha_d}\frac{\partial \boldsymbol{v}_r}{\partial t} \cong -5\alpha_d \rho_c \frac{\partial \boldsymbol{v}_r}{\partial t}. \tag{12-16}$$

Here the second form is obtained by approximating the void fraction in the slug bubble section by $\alpha_b \cong 0.8$.

The second case considered is a train of spherical-edged cylindrical bubbles, see Fig.12-1(b). Application of the Bernoulli equation

$$\frac{\partial \Phi}{\partial t} + \int \frac{dp}{\rho} + \Omega + \frac{v^2}{2} = \text{constant} \tag{12-17}$$

where Φ and Ω are respectively the velocity potential and the potential function to this geometry under a relative acceleration yields

$$\frac{\alpha_d \boldsymbol{F}_d^V}{B_d} = -5\left[0.66\alpha_d + 0.27\left(\frac{L_b - D_b}{L}\right)\right]\rho_c \frac{\partial \boldsymbol{v}_r}{\partial t} \tag{12-18}$$

where a simplification has been made on an approximation $\alpha_b \cong 0.8$ (Ishii and Mishima, 1981). For a limiting case of a train of spherical bubbles, $L_b = D_b$, the above equation reduces to

$$\frac{\alpha_d \boldsymbol{F}_d^V}{B_d} = -3.3\alpha_d \rho_c \frac{\partial \boldsymbol{v}_r}{\partial t}. \tag{12-19}$$

If $L_b >> D_b$, L_b/L can be approximated by α_d/α_b. Thus for long slug bubbles, Eq.(12-18) essentially converges to the simple solution given by Eq.(12-17). The virtual mass force for a slug flow given by Eq.(12-18) is expressed in terms of the relative acceleration in the absence of a large convective acceleration. However, if the convective acceleration can not be neglected, a special convective derivative in the form of Eq.(12-7) may be more appropriate. Thus for a general case,

$$\frac{\alpha_d \boldsymbol{F}_d^V}{B_d} = -5\left[0.66\alpha_d + 0.27\left(\frac{L_b - D_b}{L}\right)\right]\rho_c\left(\frac{D_d \boldsymbol{v}_r}{Dt} - \boldsymbol{v}_r \cdot \nabla \boldsymbol{v}_c\right). \quad (12\text{-}20)$$

This formula can also be applied to churn-turbulent flow.

Now the solutions for a dispersed flow, Eq.(12-12), and slug flow, Eq.(12-18), can be examined by introducing an induced mass coefficient C_M defined by

$$\frac{\alpha_d \boldsymbol{F}_d^V}{B_d} = -C_M \rho_c\left(\frac{D_d \boldsymbol{v}_r}{Dt} - \boldsymbol{v}_r \cdot \nabla \boldsymbol{v}_c\right) \quad (12\text{-}21)$$

where

$$C_M = \begin{cases} \dfrac{1}{2}\alpha_d \dfrac{1+2\alpha_d}{1-\alpha_d} & \text{(Bubbly flow)} \\ 5\alpha_d\left[0.66 + 0.34\left(\dfrac{1 - D_b/L_b}{1 - D_b/3L_b}\right)\right] & \text{(Slug flow).} \end{cases} \quad (12\text{-}22)$$

A plot of C_M against α_d is shown in Fig.12-2. The virtual mass force increases with an increasing void fraction of a dispersed phase due to stronger coupling between two phases. The intersection of the above two solutions occurs at the void fraction between 0.66 and 0.75. For a lower void fraction, the virtual mass force for a bubbly-flow is smaller than that for a slug-flow. This implies that the vapor phase has less resistance to an acceleration in a bubbly-flow configuration than a slug-flow configuration if $\alpha_d < 0.66$. This may also suggest that an accelerating slug flow has a tendency to disintegrate into a bubbly flow when $\alpha_d < 0.66$. For

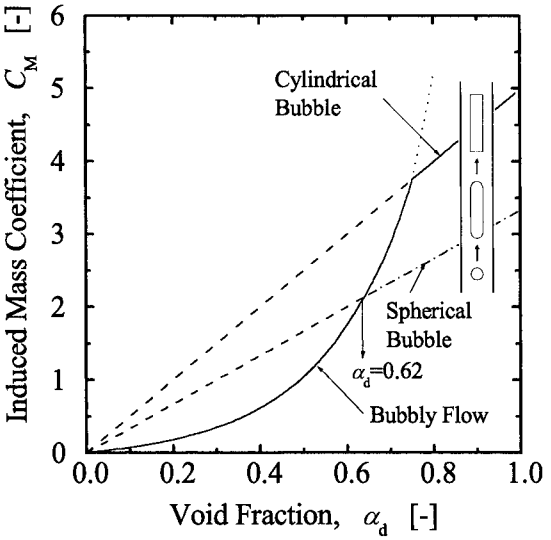

Figure 12-2. Virtual mass coefficient for dispersed and slug-flow regimes (Ishii and Mishima, 1984)

$\alpha_d > 0.66$ a slug flow should be quite stable even under a transient condition.

Due to a similarity in flow geometries, the virtual mass force for a churn-turbulent flow may be approximated by the solution for a slug flow given by Eq.(12-19). In a liquid-dispersed flow, the virtual mass force becomes considerably smaller than that in a vapor-dispersed flow. This decrease is caused by a change in the continuous phase density to be used in Eq.(12-12). By changing ρ_c from ρ_f to ρ_g, the virtual mass force for a droplet flow becomes insignificant. This also indicates that the virtual mass force should be reduced considerably in annular and annular dispersed flow.

1.2 Drag force in multiparticle system

The standard drag force acting on the particle under steady-state conditions can be given in terms of the drag coefficient C_D based on the relative velocity as

$$\boldsymbol{F}_d^D = -\frac{1}{2} C_D \rho_c \boldsymbol{v}_r |v_r| A_d \tag{12-23}$$

where A_d is the projected area of a typical particle and $\boldsymbol{v}_r$ is the relative velocity given by $\boldsymbol{v}_r = \boldsymbol{v}_d - \boldsymbol{v}_c$. Then $\boldsymbol{F}_d^D$ is related to the interfacial drag force by

$$\boldsymbol{F}_d^D = \frac{B_d \boldsymbol{M}_d^D}{\alpha_d}. \tag{12-24}$$

Hence, the portion of $\boldsymbol{M}_{id}$ represented by the drag force becomes

$$\frac{\alpha_d \boldsymbol{F}_d^D}{B_d} = -\left(\alpha_d \frac{A_d}{B_d}\right)\frac{C_D}{2}\rho_c \boldsymbol{v}_r |v_r|. \tag{12-25}$$

In what follows, a constitutive relation for the drag coefficient C_D in dispersed two-phase flows will be explained in detail starting from a single-particle system.

1.2.1 Single-particle drag coefficient

Motion of the single solid particles, drops, or bubbles in an infinite medium has been studied extensively in the past, see for example, Peebles and Garber (1953), Harmathy (1960) and Wallis (1974). In what follows we summarize these results in simple forms useful for the development of the drag correlation in multiparticle systems (Ishii and Chawla, 1979).

By denoting the relative velocity of a single particle in an infinite medium by $v_{r\infty} = v_d - v_{c\infty}$, the drag coefficient is defined by

$$C_{D\infty} = -2F_D \Big/ \left\{\rho_c v_{r\infty} |v_{r\infty}| \pi r_d^2\right\} \tag{12-26}$$

where F_D is the drag force and r_d is the radius of a particle. To calculate the drag force F_D in terms of the relative velocity, we should determine a constitutive relation for $C_{D\infty}$ independent of Eq.(12-26). For a single-particle drag correlation, two similarity parameters are important. They are the particle Reynolds number and the viscosity number

$$N_{\mathrm{Re}\infty} \equiv \frac{2r_d \rho_c |v_{r\infty}|}{\mu_c} \tag{12-27}$$

and

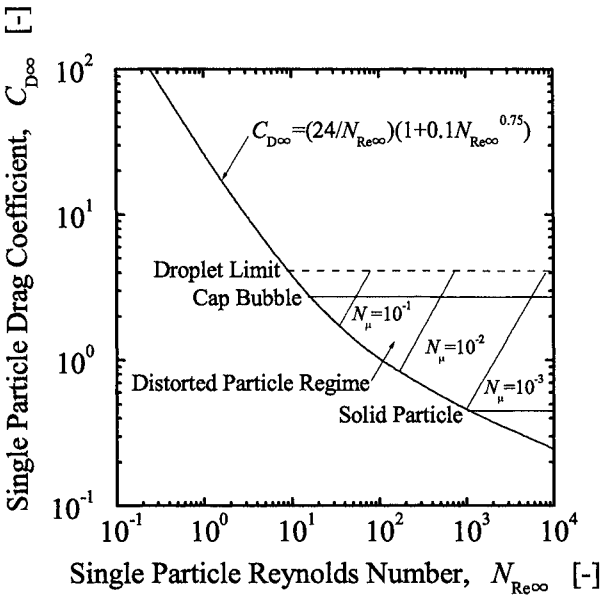

Figure 12-3. Single-particle drag coefficient (Ishii and Chawla, 1979)

$$N_\mu \equiv \frac{\mu_c}{\left(\rho_c \sigma \sqrt{\frac{\sigma}{g\Delta\rho}}\right)^{1/2}}. \qquad (12\text{-}28)$$

Extensive studies on the single particle drag show that for most cases, the drag coefficient is a function of the Reynolds number (see Fig.12-3). However, the exact functional form depends on whether the particle is a solid particle, drop, or bubble. Briefly, for a solid-spherical-particle system, we have the viscous regime, in which the Reynolds-number dependence of $C_{D\infty}$ is pronounced, and Newton's regime, in which $C_{D\infty}$ is independent of $N_{Re\infty}$. In case of a clean fluid sphere in the viscous regime, $C_{D\infty}$ can be reduced up to 33 %, in comparison with the value predicted by the correlation for solid particles. This is explained by the internal circulation within the fluid particles. However, slight amounts of impurities are sufficient to eliminate this drag reduction. Therefore, for most practical applications, the drag law in a fluid- particle system may be approximated by that for a solid-particle system up to a certain particle size. Beyond this

point, both the distortion of a particle shape and the irregular motions become pronounced. In this distorted-particle regime, $C_{D\infty}$ does not depend on the viscosity, but increases linearly with the radius of a particle. Because of the hydrodynamical instability, there is an upper limit on $C_{D\infty}$, and the particle reaches the cap bubble condition or the maximum droplet size. These regimes for the drag coefficient can be seen in Fig.12-3.

For a viscous regime, the function C_D is given by an empirical correlation as

$$C_D = \frac{24}{N_{\mathrm{Re}\infty}}\left(1 + 0.1N_{\mathrm{Re}\infty}^{0.75}\right). \tag{12-29}$$

When the Reynolds number is small ($N_{\mathrm{Re}\infty} < 1$), the above correlation essentially reduces to the well-known Stokes drag law, $C_D = 24/N_{\mathrm{Re}\infty}$. The correlation for the viscous regime indicates that the dependence of the drag coefficient on the Reynolds number decreases with increasing values of the Reynolds number.

In solid particles, the drag coefficient becomes essentially constant at approximately

$$C_{D\infty} = 0.45 \text{ for } N_{\mathrm{Re}\infty} \geq 1000. \tag{12-30}$$

This Newton's regime holds up to $N_{\mathrm{Re}\infty} = 2\times10^5$. Beyond this Reynolds number the boundary layer separation point moves from the front side to back side of a particle due to the transition of the boundary layer from laminar to turbulent. This results in sharp drop in the drag coefficient.

For fluid particles such as drops or bubbles, we have a flow regime characterized by the distortion of particle shapes and the irregular motions. In this distorted particle regime, the experimental data show that terminal velocity is independent of the particle size (see Fig.12-4). In Fig.12-4, dimensionless terminal velocity, $v_{r\infty}^*$, and reduced radius, r_d^*, are defined by $|v_{r\infty}|\left(\rho_c^2/\mu_c g\Delta\rho\right)^{1/3}$ and $r_d\left(\rho_c g\Delta\rho/\mu_c^2\right)^{1/3}$, respectively. From this, it can be seen that the drag coefficient $C_{D\infty}$ does not depend on the viscosity, but it should be proportional to the radius of the particle (Harmathy, 1960). Physically, this indicates that the drag force is governed by distortion and swerving motion of the particle, and change of the particle shape is toward an increase in the effective cross section. Therefore, $C_{D\infty}$ may be scaled by the mean radius of the particle rather than the Reynolds number (Harmathy, 1960). Then we have

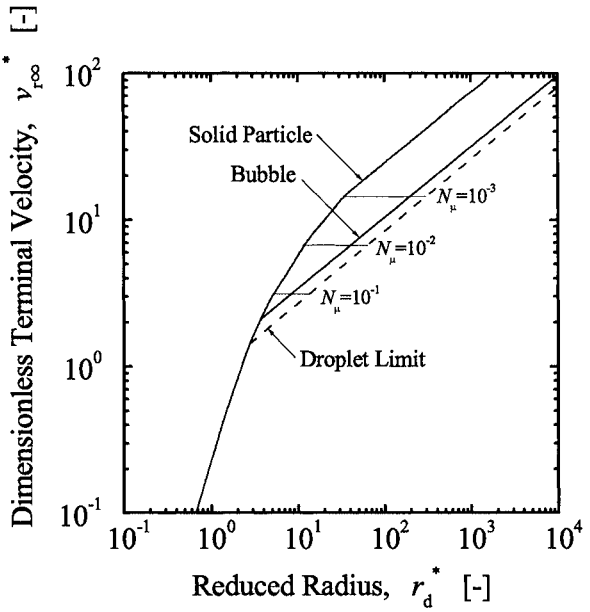

Figure 12-4. Terminal velocity for single-particle system (Ishii and Chawla, 1979)

$$C_{D\infty}=\frac{4}{3}r_d\sqrt{\frac{g\Delta\rho}{\sigma}} \text{ for } N_\mu \geq 36\sqrt{2}\left(1+0.1N_{\mathrm{Re}\infty}^{0.75}\right)/N_{\mathrm{Re}\infty}^2. \quad (12\text{-}31)$$

Here, the fluid particle size based on the terminal velocity is used.

Therefore, the flow regime transition between the viscous flow and the distorted particles flow can be given in terms of the viscosity number as shown in Figs.12-3 and 12-4. However, since in this regime the terminal velocity can be uniquely related to properties, Eq.(12-31) can be generalized in terms of the terminal velocity or the Reynolds number as

$$C_{D\infty}=\frac{\sqrt{2}}{3}N_\mu N_{\mathrm{Re}\infty}. \quad (12\text{-}32)$$

As the size of a bubble increases further, the bubble becomes spherical-cap shaped, and the drag coefficient reaches a constant value of

$$C_{D\infty} = \frac{8}{3}. \tag{12-33}$$

The transition from the distorted-bubble regime to the spherical-cap bubble regime occurs for

$$r_d = 2\sqrt{\frac{\sigma}{g\Delta\rho}}. \tag{12-34}$$

For a liquid drop, the drag coefficient may increase further according to Eq.(12-31). However, eventually a droplet becomes unstable and disintegrates into small drops. This limit can be given by the well-known Weber number criterion. By introducing the Weber number, $We \equiv 2\rho_g v_r^2 r_d / \sigma$, where v_r is the relative velocity, we can give the stability criterion approximately as $We \simeq 12$. Since the terminal velocity corresponding to Eq.(12-31) is $v_{r\infty} = \sqrt{2}\left(g\sigma\Delta\rho/\rho_g^2\right)^{1/4}$, the maximum possible drop radius is

$$r_{d\max} = 3\sqrt{\frac{\sigma}{g\Delta\rho}} \tag{12-35}$$

which corresponds to the maximum drag coefficient $C_D = 4$ for droplets. If the stability of a drop interface is governed by the Taylor instability, the characteristic drop radius is given by

$$r_{d\max} = \sqrt{\frac{\sigma}{g\Delta\rho}} \tag{12-36}$$

which may be a more practical upper limit of the drop size. It is also noted that in highly turbulent flow (Hinze, 1959) or under pressure shock conditions (Dinh et al., 2003; Theofanous et al., 2004) the stability limit Weber number can be much smaller than 12.

The cap bubble maintains a certain regular shape with the wake angle of about 50°, however there is also a maximum stable cap bubble diameter (Grace et al., 1978; Clift et al., 1978; Kocamstafaogullari et al., 1984; Miller, 1993). This instability is shown in Fig.12-5. Kocamustafaogullari et al. (1984) used the stability analysis based on the Kelvin-Helmholtz instability along the cap bubble surface. By comparing the surface wave residence time and the time for the wave amplitude to grow to the order of the magnitude of the bubble size, the stability criterion has been obtained. For most practical

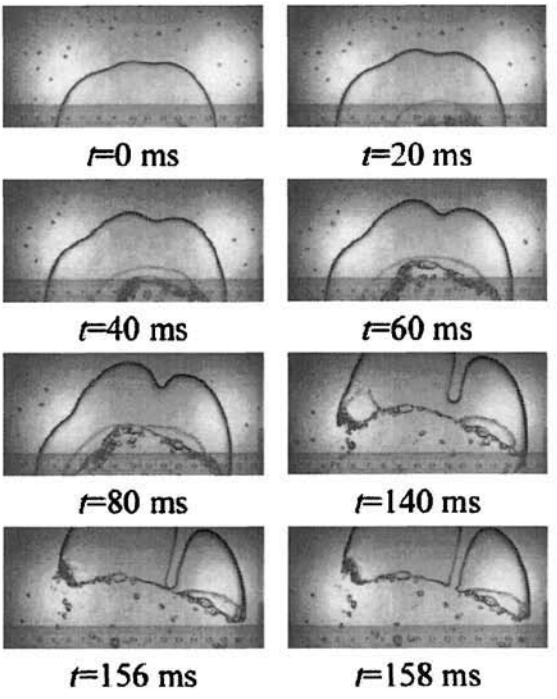

Figure 12-5. Large bubble breakup due to instability (500 frames/s)

cases, this stability limit can be approximated by

$$r_{cap,\max} = 20\sqrt{\frac{\sigma}{g\Delta\rho}}. \tag{12-37}$$

This result is significant because it defines the boundary between the smaller pipe where slug flow is possible and the larger pipe where slug flow cannot be formed due to the instability of the Taylor bubbles. For a pipe diameter $D < 2r_{cap,\max}\left(= 40\sqrt{\sigma/g\Delta\rho}\right)$ a stable slug flow can be formed. However for $D >> 2r_{cap,\max}$ bubbly flow is followed by cap-turbulent flow where multiple interacting cap bubbles exist at higher gas flux.

Using the above drag coefficient, we can obtain the terminal velocity in infinite media by balancing the pressure, gravity, and drag forces. The results are summarized in Fig.12-4 for various particles and flow regimes.

1.2.2 Drag coefficient for dispersed two-phase flow

A. Effects of Particles and Flow Regimes

In the preceding section it has been shown that the drag correlation for a single-particle system depends not only on the flow regimes but also on the nature of the particles; namely, solid particle, drop or bubble. Therefore, for a multiparticle system, these differences are also expected to play central roles in determining the drag correlation. In the present study, the multiparticle drag correlation is developed in parallel with the single-particle system by considering the following flow regimes

Solid-particle system
- Viscous regime
- Newton's regime

Fluid-particle system
- Viscous regime
- (Undistorted-particle regime)
- Distorted-particle regime
- Churn-turbulent-flow regime
- Slug-flow regime

In the viscous regime, distortions of fluid particles are negligible. Therefore, for this regime, solid- and fluid-particle systems are considered together. Although small differences exist between these two systems due to the surface flow, for most cases these differences can be neglected (Clift et al., 1978). The other flow regimes are analyzed separately because of significant differences in the flow around the particles and the motions of the interfaces.

B. Viscous Regime (Undistorted-Particle Regime)

This regime is characterized by the strong effect of viscosity on the particle motion. For a fluid-particle system, this regime occurs only when particle shapes are not distorted due to interfacial instabilities or turbulent fluid motion. To develop a multiparticle drag correlation, several similarity hypotheses are introduced. First, it is assumed that the drag coefficient in the viscous regime can be given as a function of the particle Reynolds number. Thus,

$$C_D = C_D(N_{\mathrm{Re}}) \tag{12-38}$$

where the Reynolds number is defined in terms of the mixture viscosity μ_m as

$$N_{\mathrm{Re}} \equiv \frac{2\rho_c |v_r| r_d}{\mu_m}. \tag{12-39}$$

The introduction of the drag coefficient, Eq.(12-23), and the use of Eq. (12-38) are based on the assumption that the resistance to particle motion in a two-phase mixture can be evaluated by considering the local resistance to the shearing caused by the relative motion between the representative particle and the surrounding fluid. The effect of the other particles on the drag force arises from the resistance of the particle to the deformation of the flow field. Since the particles are more rigid than the fluid against deformations, the particles will impose a system of forces that will react upon the fluid. As a result of additional stresses, the original particles see an increase in the resistance to its motion, which appears to it as arising from an increase of viscosity.

Consequently, in analyzing the motion of the suspended particles, mixture viscosity should be used (Burgers, 1941; Zuber, 1964a). It is expected that the mixture viscosity is a function of concentration, fluid viscosity and particle viscosity. The viscosity of the dispersed phase takes account of the mobility of the interface and is the measure of the resistance to the particle-material motion along the interface. The effect of the particle collisions may be indirectly reflected in the mixture viscosity through the void fraction. Furthermore, for a fluid-particle system, the surface tension should have an effect on the particle collisions and coalescences. This is particularly important in determining the flow-regime transitions.

In the present analysis, we extend the linear correlation (Taylor, 1932) for the mixture viscosity for fluid particles along the power relation (Roscoe, 1952) for solid particles based on the maximum packing α_{dm}. Taylor's viscosity model for a fluid-particle system is given by

$$\frac{\mu_m}{\mu_c} = 1 + 2.5\alpha_d \frac{\mu_d + 0.4\mu_c}{\mu_d + \mu_c} \tag{12-40}$$

which is applicable only for $\alpha_d << 1$. The simple power-law viscosity model for a solid-particle system is given by

$$\frac{\mu_m}{\mu_c} = \left(1 - \frac{\alpha_d}{\alpha_{dm}}\right)^{-2.5\alpha_{dm}} . \tag{12-41}$$

This shows that the viscosity of the mixture increases rapidly near the maximum packing. Note also that linear expansion of Eq.(12-41) at small α_d is $\mu_m/\mu_c = 1 + 2.5\alpha_d$, which is similar to Eq.(12-40). The maximum packing α_{dm} for solid-particle systems ranges from 0.5 to 0.74. However, $\alpha_{dm} = 0.62$ suffices for most of the practical cases. For a bubbly flow, theoretical α_{dm} can be much higher because of the deformation of bubbles. In the absence of turbulent motions and particle coalescences, the void fraction in a fluid-particle system can be as high as 0.95. By taking α_{dm} to be unity, we can include these foam or dense packing regimes in the analysis. Therefore, for fluid-particle systems, we take $\alpha_{dm} = 1$. Combining the above two expressions produces the following model for both a solid-particle system and a fluid-particle system at all concentrations

$$\frac{\mu_m}{\mu_c} = \left(1 - \frac{\alpha_d}{\alpha_{dm}}\right)^{-2.5\alpha_{dm}(\mu_d + 0.4\mu_c)/(\mu_d + \mu_c)} . \tag{12-42}$$

Figure 12-6 compares this mixture-viscosity model to the various existing models for solid-particle systems (Eilers, 1941; Roscoe, 1952; Brinkman, 1952; Frankel and Acrivos, 1967; Landel et al., 1965; Thomas, 1965). Note that, for a solid particle system, μ_d approaches ∞. Thus, if we take the limit of Eq.(12-42), the viscosity-ratio term becomes unity and the correlation reduces to the power law, Eq.(12-41). By including the effect of viscosity of the dispersed phase in the correlation, this model has the advantage over the conventional correlations, because it is not limited to particulate flows, but can also be applied to droplet and bubble flows.

Using the recommended values for maximum packing, we can approximate the mixture viscosity by a simple power law given by

$$\mu_m/\mu_c = (1 - \alpha_d)^{-n} \tag{12-43}$$

$$\text{where} \quad n = \begin{cases} 1 & \text{Bubbly flow} \\ 1.75 & \text{Drops in liquid} \\ 2.5 & \text{Drops in gas, particulate flow.} \end{cases} \tag{12-44}$$

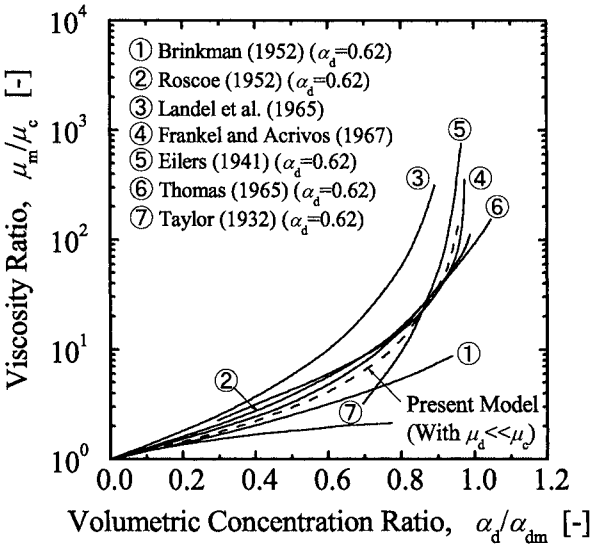

Figure 12-6. Comparison of present mixture-viscosity model and existing models for solid-particle system (Ishii and Chawla, 1979)

The expression for the solid-particle system is applicable only up to a moderate value of α_d. These relations are shown in Fig.12-7.

The second similarity hypothesis introduced in the analysis is that, in the viscous regime, a complete similarity exists between a single-particle system and a multi-particle system. Therefore, the multiparticle drag coefficient C_D has exactly the same functional form in terms of N_{Re} as $C_{D\infty}$ in terms of $N_{\mathrm{Re}\infty}$ given by Eq.(12-29). Then $C_D = C_{D\infty}\left(N_{\mathrm{Re}}\right)$ or

$$C_D = \frac{24}{N_{\mathrm{Re}}}\left(1 + 0.1 N_{\mathrm{Re}}^{0.75}\right). \tag{12-45}$$

The relation given by Eq.(12-45) is shown in Fig.12-8. This correlation indicates that the drag coefficient increases with an increasing volumetric concentration α_d. This trend is clearly shown in Fig.12-9 for a solid-particle system by comparing single- and multi-particle systems.

The similarity criterion given by $C_D\left(N_{\mathrm{Re}}\right) = C_{D\infty}\left(N_{\mathrm{Re}}\right)$ with the Reynolds number based on mixture viscosity is first introduced for solid-particles system in the Stokes regime (Hawksley, 1951; Zuber, 1964a). Note that the present model is not limited to a solid-particle system or to the

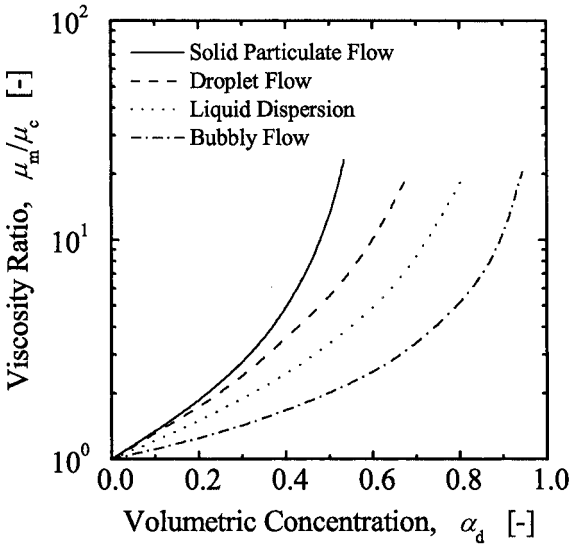

Figure 12-7. Mixture viscosity for various systems (Ishii and Chawla, 1979)

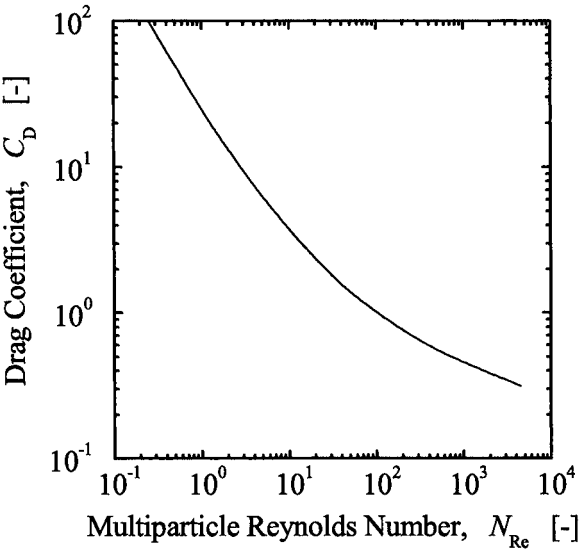

Figure 12-8. Drag coefficient in viscous regime (Ishii and Chawla, 1979)

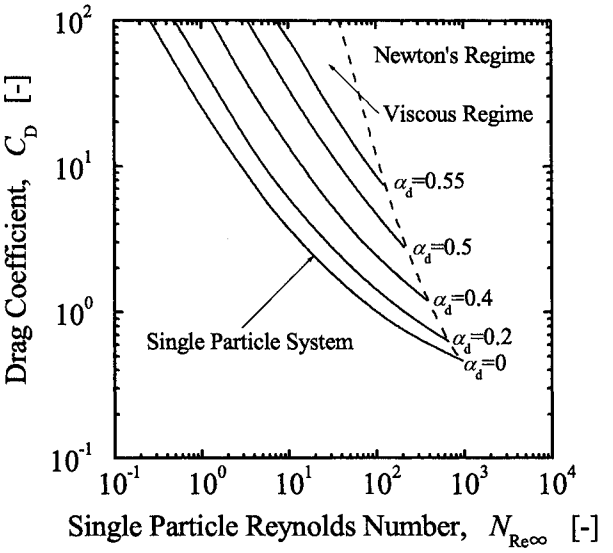

Figure 12-9. Effect of concentration on drag coefficient in viscous regime (Ishii and Chawla, 1979)

Stokes regime, however, because of the use of the generalized drag law and the applicability of the mixture-viscosity model to fluid-particle systems.

C. Newton's Regime

In Newton's regime, a vortex system develops behind a particle and its departure creates a large wake region. The drag force is mainly determined by the eddies generated by a separation of the flow. Hence, for a single-particle system, the drag force is approximately proportional to the inertia force and the drag coefficient can be considered constant.

For a multiparticle system, the drag coefficient in Newton's regime is assumed not to depend on the Reynolds number but on the void fraction. The effect of the other particles should be through α_d. Hence,

$$C_D = 0.45E(\alpha_d). \tag{12-46}$$

The function $E(\alpha_d)$ can be obtained by considering a special case of the terminal velocity in an infinite medium. From a force balance between gravity, pressure, and drag forces, we have

$$v_r |v_r| = \frac{8}{3} \frac{r_d}{C_D \rho_c} (\rho_c - \rho_d) g (1 - \alpha_d). \tag{12-47}$$

For a single-particle system, this reduces to

$$v_{r\infty} |v_{r\infty}| = \frac{8}{3} \frac{r_d}{C_{D\infty} \rho_c} (\rho_c - \rho_d) g. \tag{12-48}$$

By comparing a multiparticle system to a single-particles system having the same particles size, we have

$$\frac{v_r}{v_{r\infty}} = \sqrt{\frac{C_{D\infty}(N_{\mathrm{Re}\infty})(1 - \alpha_d)}{C_D(N_{\mathrm{Re}})}}. \tag{12-49}$$

Since Reynolds numbers can be a function of the velocities, Eq.(12-49) is an implicit equation for the terminal velocity v_r. If we consider the viscous-regime drag laws given by Eqs.(12-29) and (12-45), Eq.(12-49) becomes

$$\frac{v_r}{v_{r\infty}} = \frac{\mu_c}{\mu_m} (1 - \alpha_d) \frac{1 + 0.1 N_{\mathrm{Re}\infty}^{0.75}}{1 + 0.1 N_{\mathrm{Re}}^{0.75}}. \tag{12-50}$$

The limiting case of $r_d \to 0$ (or $N_{\mathrm{Re}}, N_{\mathrm{Re}\infty} \to 0$) is

$$\lim_{r_d \to 0} \frac{v_r}{v_{r\infty}} = \frac{\mu_c}{\mu_m} (1 - \alpha_d). \tag{12-51}$$

For $r_d \to \infty$ (or $N_{\mathrm{Re}}, N_{\mathrm{Re}\infty} \to \infty$),

$$\lim_{r_d \to \infty} \frac{v_r}{v_{r\infty}} = \left(\frac{\mu_c}{\mu_m} \right)^{1/7} (1 - \alpha_d)^{4/7}. \tag{12-52}$$

By interpolating between these limits in view of Eq.(12-50), we obtain an approximate explicit solution for v_r given by

$$\frac{v_r}{v_{r\infty}} = (1 - \alpha_d) \frac{\mu_c}{\mu_m} \frac{1 + 0.1 N_{\mathrm{Re}\infty}^{0.75}}{1 + 0.1 N_{\mathrm{Re}\infty}^{0.75} \left[\sqrt{1 - \alpha_d}\, \mu_c / \mu_m \right]^{6/7}}. \tag{12-53}$$

Since the terminal velocity $v_{r\infty}$ is uniquely related to the Reynolds number by Eq.(12-48), however, $N_{\mathrm{Re}\infty}$ can be replaced by a radius of a particles. Thus,

$$\frac{v_r}{v_{r\infty}} \simeq (1-\alpha_d)\frac{\mu_c}{\mu_m}\frac{1+\psi(r_d^*)}{1+\psi(r_d^*)\left[\sqrt{1-\alpha_d}\mu_c/\mu_m\right]^{6/7}} \tag{12-54}$$

where

$$\begin{cases} r_d^* = r_d\left(\rho_c g\Delta\rho/\mu_c^2\right)^{1/3} \\ \text{and} \\ \psi(r_d^*) = 0.55\left[\left(1+0.08r_d^{*3}\right)^{4/7}-1\right]^{0.75}. \end{cases} \tag{12-55}$$

For a single-particles system, the transition from the viscous regime to Newton's regime occurs at $r_d^* = 34.65$ (or $N_{\mathrm{Re}\infty} \simeq 990$). At this particles size, Eq.(12-46) reduces to

$$\frac{v_r}{v_{r\infty}} = (1-\alpha_d)\frac{\mu_c}{\mu_m}\frac{18.67}{1+17.67\left[\sqrt{1-\alpha_d}\mu_c/\mu_m\right]^{6/7}}. \tag{12-56}$$

This equation is valid up to the transition from the viscous regime to Newton's regime in a multiparticle system. Therefore, at this transition point the drag-coefficient ratio can be calculated from Eqs.(12-49) and (12-56) as

$$C_D = C_{D\infty}\left(\frac{1+17.67\left(\sqrt{1-\alpha_d}\mu_c/\mu_m\right)^{6/7}}{18.67\sqrt{1-\alpha_d}\mu_c/\mu_m}\right)^2 \tag{12-57}$$

where $C_{D\infty} = 0.45$ at $r_d^* = 34.65$. In view of Eq.(12-42) with $\alpha_{dm} = 0.62$, we obtain

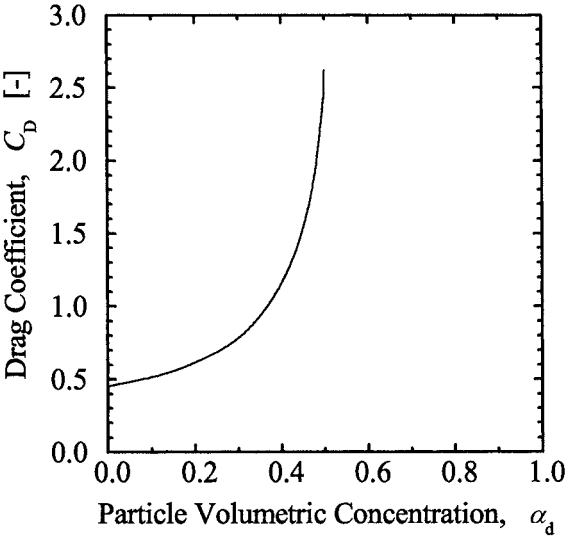

Figure 12-10. Drag coefficient for Newton's regime (Ishii and Chawla, 1979)

$$C_D = 0.45\left(\frac{1+17.67\left[f(\alpha_d)\right]^{6/7}}{18.67 f(\alpha_d)}\right)^2 \qquad (12\text{-}58)$$

$$\text{with } f(\alpha_d) \equiv (1-\alpha_d)^{0.5}\left(1-\frac{\alpha_d}{0.62}\right)^{1.55}.$$

The increase of the drag coefficient with increasing volumetric concentration α_d is shown in Fig.12-10 by plotting Eq.(12-58). This implies that the equilibrium relative velocity generally decreases with increases in the concentration due to stronger coupling between phases.

D. Distorted-fluid-particle Regime

In the distorted-fluid-particle regime, the single particle drag coefficient depends only on the particle radius and fluid properties and not on the velocity or the viscosity, namely, $C_{D\infty} = \left(4/3\right) r_d \sqrt{g\Delta\rho/\sigma}$, as discussed by Harmathy (1960). Thus, for a particle of a fixed diameter, $C_{D\infty}$ becomes constant. In considering the drag coefficient for a multiparticle system with the same radius, we must take into account the restrictions imposed by the

existence of other particles on the flow field. Therefore, C_D is expected to be different from $C_{D\infty}$, in this regime.

Because of the strong contribution of the turbulent eddies on the wake region, a particle sees the increased drag due to other particles in essentially similar ways as in the Newton's regime for a solid-particle system where $C_{D\infty}$ is also constant under a wake-dominated flow condition. Hence, we postulate that, regardless of the differences in $C_{D\infty}$ in these regimes, the effect of increased drag in the distorted-fluid-particle regime can be predicted by an expression similar to that in the Newton's regime.

Under this assumption, Eq.(12-57) can be used with a proper expression for $C_{D\infty}$ given by Eq. (12-43). Thus,

$$C_D = \frac{\sqrt{2}}{3} N_\mu N_{\mathrm{Re}\infty} \left(\frac{1 + 17.67 \left(\sqrt{1-\alpha_d}\, \mu_c / \mu_m \right)^{6/7}}{18.67 \sqrt{1-\alpha_d}\, \mu_c / \mu_m} \right)^2 . \tag{12-59}$$

In view of the approximation given by Eq.(12-43), the above correlation reduces to

$$C_D = \frac{\sqrt{2}}{3} N_\mu N_{\mathrm{Re}\infty} \left(\frac{1 + 17.67 \left(1-\alpha_d\right)^{6(n+0.5)/7}}{18.67 \left(1-\alpha_d\right)^{n+0.5}} \right)^2 \tag{12-60}$$

where n is given by Eq.(12-44). Thus, for a bubbly flow ($n = 1$),

$$C_D = \frac{\sqrt{2}}{3} N_\mu N_{\mathrm{Re}\infty} \left(\frac{1 + 17.67 \left(1-\alpha_d\right)^{1.3}}{18.67 \left(1-\alpha_d\right)^{1.5}} \right)^2 . \tag{12-61}$$

For a droplet-liquid flow ($n = 1.75$)

$$C_D = \frac{\sqrt{2}}{3} N_\mu N_{\mathrm{Re}\infty} \left(\frac{1 + 17.67 \left(1-\alpha_d\right)^{1.9}}{18.67 \left(1-\alpha_d\right)^{2.3}} \right)^2 . \tag{12-62}$$

For a droplet-gas flow ($n = 2.5$)

$$C_D = \frac{\sqrt{2}}{3} N_\mu N_{\mathrm{Re}\infty} \left(\frac{1 + 17.67 \left(1-\alpha_d\right)^{2.6}}{18.67 \left(1-\alpha_d\right)^{3}} \right)^2 . \tag{12-63}$$

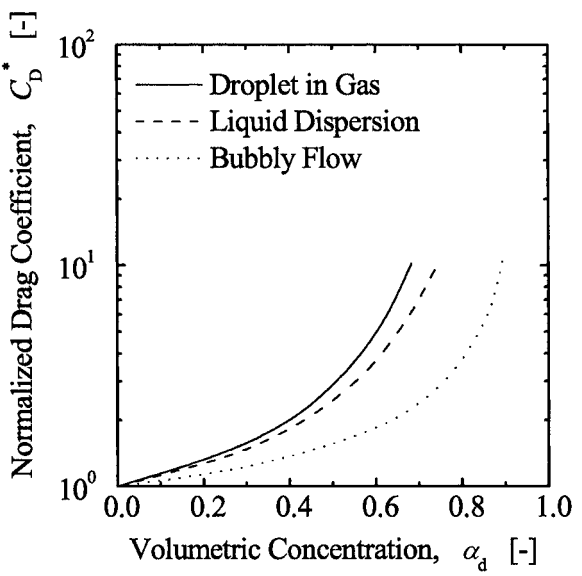

Figure 12-11. Drag coefficient in distorted-particle regime (Ishii and Chawla, 1979)

The above three correlations are shown in Fig.12-11. The form of the correlations indicates that the momentum coupling between phases increases with increasing particle concentration as in the case for Newton's regime.

E. Churn-turbulent-flow Regime

As the radius of the fluid particle is further increased, the wake and bubble boundary layer can overlap due to the formation of large wake regions. In other words, a particle can influence both the surrounding fluid and other particles directly. Hence, the entrainment of a particle in a wake of other particles becomes possible. This flow regime is known as the churn-turbulent flow regime and is commonly observed in bubbly flows. In the existence of sufficient turbulent motions in the continuous phase, the transition from the distorted-particle regime to the churn-turbulent flow regime occurs at the particle concentration around 0.3. This criterion for the transition can be applied to most forced-convection two-phase flows. In a batch process, however, detailed coalescence mechanisms and surface contaminations become important in determining the transition criterion.

In the churn-turbulent flow regime, a typical particle moves with respect to the average volumetric flux j rather than the average velocity of a continuous phase due to the hydrodynamic conditions discussed above.

Hence, the reference velocity in the definitions of the drag coefficient and the drag-similarity law should be the drift velocity rather than the relative velocity. Hence, the drag force should be given by

$$F_D = -\frac{1}{2} C'_D \rho_c V_{dj} \left| V_{dj} \right| \pi r_d^2. \tag{12-64}$$

Here the drift velocity V_{dj} is the relative velocity of the dispersed phase with respect to the center-of-volume velocity of a mixture. It can also be related to the true relative velocity between phases by

$$V_{dj} = v_d - j = (1 - \alpha_d) v_r \tag{12-65}$$

where the total flux j (center-of-volume velocity) is given by

$$j = \alpha_d v_d + (1 - \alpha_d) v_c. \tag{12-66}$$

In a churn-turbulent-flow regime, some particles should have reached the distortion limit corresponding to the cap-bubble transition or the droplet disintegration. This limit can be given as an extension of the Weber number criterion (Wallis, 1969) by using the drift velocity as a reference velocity in the following form

$$\frac{2\rho_c V_{dj}^2 r_d}{\sigma} = \begin{cases} 8 & \text{(bubble)} \\ 12 & \text{(droplet).} \end{cases} \tag{12-67}$$

Due to the entrainment of particles in the wake of other larger particles and the coalescence and disintegration caused by the turbulence, the average motion of the dispersed phase is mainly governed by those particles that satisfy the Weber-number criterion. Hence, the effective drag coefficient is given by $C'_D = 8/3$. If we recast the above drag-force expression based on the drift velocity to the conventional one based on the relative velocity, we obtain

$$F_D = -\frac{8}{3}(1 - \alpha_d)^2 \frac{\rho_c v_r \left| v_r \right| \pi r_d^2}{2} \tag{12-68}$$

where the reference r_d for the drag-force expression is given by $r_d = (4 \text{ or } 6)\sigma \Big/ \left[\rho_c v_r^2 (1 - \alpha_d)^2\right]$, because these particles govern the relative

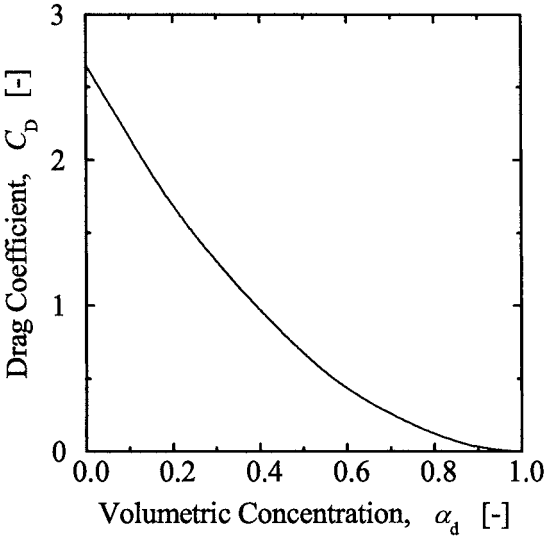

Figure 12-12. Drag coefficient for churn-turbulent flow (Ishii and Chawla, 1979)

motion. The above equation implies that the apparent drag coefficient based on the true relative velocity between phases should be given by

$$C_D = \frac{8}{3}(1-\alpha_d)^2. \tag{12-69}$$

The form of Eq.(12-69) indicates that the drag coefficient decreases as the particle volumetric concentration increases, as shown in Fig.12-12. Therefore, the effect of α_d on C_D in the churn-turbulent-flow regime is opposite that in the other flow regimes. This peculiar trend can be explained by the effect of the entrainment of other particles behind a wake of larger particles. This entrainment promotes the channeling of the dispersed phase without increasing the drag force. As the volumetric concentration increases, the interaction among particles increases in the direction of reducing the drag force.

F. Slug-flow Regime

One of the limiting cases of the dispersed two-phase flow in a confined channel is a slug flow. When the volume of a bubble becomes very large, the shape of the bubble is significantly deformed to fit the channel geometry. The diameters of the bubbles become nearly that of the pipe with a thin

liquid film separating the bubbles from the wall. The bubbles have an elongated bullet form with a cap-shaped nose. The motion of these bubbles in relatively inviscid fluids can be studied by using a potential flow analysis around a nose of a single bubble. Hence, Dumitrescu (1943) analytically obtained the rise velocity to be

$$v_{r\infty} = 0.35\sqrt{gD\Delta\rho/\rho_c} \tag{12-70}$$

where D is the hydraulic diameter. This result is also in good agreement with the experimental data of Dumitrescu (1943) and White and Beardmore (1962).

In a flowing system with chains of bubbles, the effect of the concentration and velocity profile should be considered. In general, the core velocity is higher than the cross-sectional area-averaged velocity due to the velocity profile. Therefore, the relative velocity based on the average velocities is larger than the local relative velocity in the core. This effect, known as the distribution-parameter effect, was studied extensively by Bankoff (1960), Zuber and Findlay (1965), and Ishii (1977) among others. When the average velocities are used, the results of Nicklin et al. (1962) and Neal (1963) show that

$$v_d - \langle j \rangle = 0.2\langle j \rangle + 0.35\sqrt{gD\Delta\rho/\rho_c}. \tag{12-71}$$

Here the left-hand side is the drift velocity of a bubble, namely, $\overline{V_{dj}} = v_d - \langle j \rangle$. The above equation can be rewritten as

$$v_d - j_{core} = 0.35\sqrt{gD\Delta\rho/\rho_c} \tag{12-72}$$

where $j_{core} \equiv 1.2\langle j \rangle$ and j_{core} may be considered as the local total flux in the core. In this case, $v_d - j_{core}$ is the local drift velocity in the core. In view of the relation given by Eq.(12-65), the local relative velocity v_r should satisfy

$$(1-\alpha_d)v_r = 0.35\sqrt{gD\Delta\rho/\rho_c} \tag{12-73}$$

which agrees with Dumitrescu's result at $\alpha_d \to 0$.

By limiting our discussion to the local drag coefficient, we can recast the above semiempirical result into a correlation for a drag coefficient in the slug-flow regime. In view of Eqs.(12-73) and (12-47), we obtain

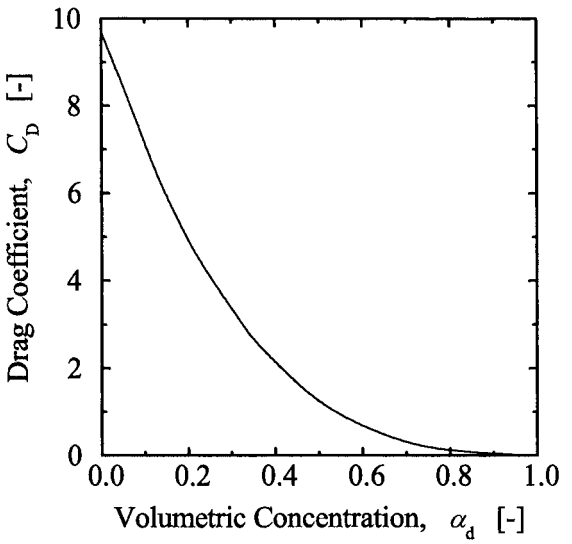

Figure 12-13. Drag coefficient for slug flow (Ishii and Chawla, 1979)

$$C_D = 10.9\frac{2r_d}{D}(1-\alpha_d)^3. \tag{12-74}$$

For most practical applications, $2r_d/D$ can be approximated by 0.9. Then,

$$C_D \simeq 9.8(1-\alpha_d)^3. \tag{12-75}$$

This correlation shows that the drag coefficient decreases with increase in the volumetric concentration, as shown in Fig.12-13. This clearly indicates the effect of the wake and channeling in the chains of bubbles in the slug-flow regime. Furthermore, C_D does not depend on the fluid properties. These two characteristics are similar to those of the churn-turbulent-flow regime. Table 12-1 summarizes the present drag coefficient in various flow regimes.

1.3 Other forces

In addition to the standard drag force and the virtual mass force, some forces such as the lift force and the turbulent dispersion forces are also

Table 12-1. Local drag coefficient in multiparticle system (Ishii and Chawla, 1979)

	Fluid Particle System			Solid Particle System
	Bubble in Liquid	Drop in Liquid	Drop in Gas	
Viscosity Model	$\frac{\mu_m}{\mu_c} = \left(1 - \frac{\alpha_d}{\alpha_{dm}}\right)^{-2.5\alpha_{dm}\mu^*}$, $\mu^* \equiv \frac{\mu_d + 0.4\mu_c}{\mu_d + \mu_c}$			
Max. Packing α_{dm}	~ 1	~ 1	$0.62 \sim 1$	~ 0.62
μ^*	0.4	~ 0.7	1	1
μ_m/μ_c	$(1-\alpha_d)^{-1}$	$(1-\alpha_d)^{-1.75}$	$\sim (1-\alpha_d)^{-2.5}$	$\left(1 - \frac{\alpha_d}{0.62}\right)^{-1.55}$
Stokes Regime C_D	$C_D = \frac{24}{N_{\mathrm{Re}}}$ where $N_{\mathrm{Re}} \equiv \frac{2r_d\rho_c v_r}{\mu_m}$			
Viscous Regime C_D	$C_D = \frac{24\left(1 + 0.1N_{\mathrm{Re}}^{0.75}\right)}{N_{\mathrm{Re}}}$			
Newton's Regime C_D	———			$C_D = 0.45\left\lvert\frac{1+17.67\{f(\alpha_d)\}^{6/7}}{18.67 f(\alpha_d)}\right\rvert^2$ where $f(\alpha_d) = \sqrt{1-\alpha_d}\left(\frac{\mu_c}{\mu_m}\right)$
Distorted Particle Regime C_D	$C_D = \frac{4}{3} r_d \sqrt{\frac{g\Delta\rho}{\sigma}}\left\lvert\frac{1+17.67\{f(\alpha_d)\}^{6/7}}{18.67 f(\alpha_d)}\right\rvert^2$ $f(\alpha_d) = (1-\alpha_d)^{1.5} \quad (1-\alpha_d)^{2.25} \quad (1-\alpha_d)^3$			
Churn-turbulent Flow Regime C_D	$C_D = \frac{8}{3}(1-\alpha_d)^2$			
Slug Flow C_D	$C_D = 9.8(1-\alpha_d)^3$			

considered in a multidimensional two-phase flow analysis. As can be seen from Eq.(12-3), these forces are customarily added to the standard drag force and the virtual mass force linearly. In an actual two-phase flow, a wake behind a bubble may completely change the liquid turbulence structure, and thus the lift force may closely be coupled with the turbulence-induced force. Since the lift force and other lateral forces are small and may closely be coupled each other, it is difficult to identify each force experimentally. Therefore, it may be controversial that such forces can be added to the standard drag force and the virtual mass force linearly. In the present status of the development, constitutive equations for some forces are proposed

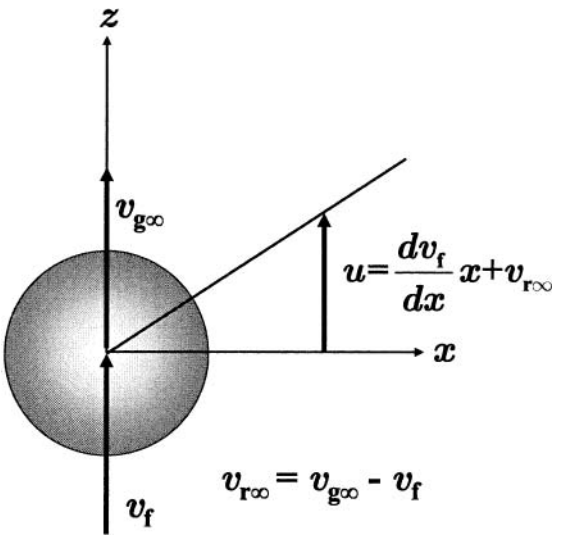

Figure 12-14. Schematic diagram of a particle in a shear flow

based on a speculation, and the applicable flow ranges of the constitutive equations are not given clearly. Thus, unlike the standard drag force, the constitutive equations for such lateral forces have not been well-developed. Nevertheless, these forces play an important role in predicting three-dimensional bubble distribution. In what follows, some constitutive equations for lift force and turbulent dispersion force, which are often used in a multidimensional two-phase flow analysis, are explained briefly. A review of lift force modeling can also be found in Akiyama and Aritomi (2002).

1.3.1 Lift force

Consider a single spherical particle moving through a very viscous liquid relative to a uniform simple shear, see Fig.12-14. Then, the particle experiences a lift force, $\boldsymbol{F}_{d\infty}^{LS-V}$, perpendicular to the flow direction as (Saffman, 1965)

$$\boldsymbol{F}_{d\infty}^{LS-V} = -6.46\mu_f \nu_f^{-1/2} v_{r\infty} r_d^2 \left|\frac{dv_f}{dx}\right|^{1/2} \mathrm{sgn}\left(\frac{dv_f}{dx}\right)\boldsymbol{e}_x. \qquad (12\text{-}76)$$

For positive relative velocity and velocity gradient ($v_{r\infty} > 0$ and $dv_f/dx > 0$), the lift force pushes the particle towards the negative x direction.

Consider a single spherical particle placed in a weak shear flow of an inviscid flow. Then, the particle experiences a lift force, $\boldsymbol{F}_{d\infty}^{LS-I}$, as (Auton, 1987)

$$\boldsymbol{F}_{d\infty}^{LS-I} = -0.5\rho_f \frac{4}{3}\pi r_d^3 \boldsymbol{v}_{r\infty} \times \mathrm{rot}\boldsymbol{v}_f. \tag{12-77}$$

Mei and Klausner (1994) proposed an expression for the shear lift force at finite Reynolds number and finite shear by interpolating Saffman's result at small $N_{\mathrm{Re}\infty}$ (1965) and Auton's result at large $N_{\mathrm{Re}\infty}$ (1987). They also considered the extension of the lift force to a fluid sphere. The proposed lift force model is given by

$$\boldsymbol{F}_{d\infty}^{LS} = -f\left(G_{s\infty}, N_{\mathrm{Re}\infty}\right)\frac{1}{2}\pi r_d^2 \rho_f v_{r\infty}^2 \,\mathrm{sgn}\left(v_{r\infty}\frac{dv_f}{dx}\right)\boldsymbol{e}_x \tag{12-78}$$

$$f\left(G_{s\infty}, N_{\mathrm{Re}\infty}\right) = G_{s\infty}^{1/2}\left[\left\{\frac{1.72J\left(\sqrt{2G_{s\infty}/N_{\mathrm{Re}\infty}}\right)}{N_{\mathrm{Re}\infty}^{1/2}}\right\}^2 + \frac{16}{9}G_{s\infty}\right]^{1/2} \tag{12-79}$$

$$J\left(\sqrt{2G_{s\infty}/N_{\mathrm{Re}\infty}}\right) \approx 0.6765\left[1+\tanh\left\{2.5\left(\log_{10}\sqrt{2G_{s\infty}/N_{\mathrm{Re}\infty}}+0.191\right)\right\}\right] \times\left[0.667+\tanh\left\{6\left(\sqrt{2G_{s\infty}/N_{\mathrm{Re}\infty}}-0.32\right)\right\}\right] \tag{12-80}$$

$$G_{s\infty} \equiv \left|\frac{r_d}{v_{r\infty}}\frac{dv_f}{dx}\right|. \tag{12-81}$$

The Reynolds number of a single particle system, $N_{\mathrm{Re}\infty}$, is defined by Eq.(12-27).

In the 1980s and 1990s, extensive experiments were performed to identify important parameters to determine the lateral bubble migration characteristics. The experiments showed that relatively small and large bubbles tend to migrate toward a channel wall and center, respectively (Zun, 1988; Liu, 1993; Hibiki and Ishii, 1999). A numerical simulation of single bubbles in a Poiseuille flow (Tomiyama et al., 1993; 1995) suggested that the bubble migration toward the pipe center was related closely to a slanted wake behind a deformed bubble. Thus, it has been indicated that the bubble size and complex interaction between a bubble wake and a shear field around the bubble play an important role in the lateral bubble migration (Serizawa and Kataoka, 1988; 1994). Tomiyama et al. (2002) measured bubble trajectories of single air bubbles in simple shear flows of glycerol-water solutions to evaluate transverse lift force acting on single bubbles. Based on the experimental result, they assumed the lift force caused by the slanted wake has the same functional form as that of the shear-induced lift force, and proposed an empirical correlation of the lift coefficient.

Hibiki and Ishii proposed the correlation of the lift coefficient based on the shear-lift force model of Mei and Klausner (1994) and the concept of the lift force caused by slanted wake, $\boldsymbol{F}_{d\infty}^{LW}$, (Tomiyama et al., 2002) such as the functional form of $\boldsymbol{F}_{d\infty}^{LW}$ to be the same as that of $\boldsymbol{F}_{d\infty}^{LS}$. Thus, the net transverse lift force, $\boldsymbol{F}_{d\infty}^{LT}$, is given by

$$\begin{aligned}\boldsymbol{F}_{d\infty}^{LT} &= \boldsymbol{F}_{d\infty}^{LS} + \boldsymbol{F}_{d\infty}^{LW} \\ &= -f\left(G_{s\infty}, N_{\mathrm{Re}\infty}\right)\frac{1}{2}\pi r_d^2 \rho_f v_{r\infty}^2 \operatorname{sgn}\left(v_{r\infty}\frac{dv_f}{dx}\right)\boldsymbol{e}_x \\ &\quad -C_{LW} f\left(G_{s\infty}, N_{\mathrm{Re}\infty}\right)\frac{1}{2}\pi r_d^2 \rho_f v_{r\infty}^2 \operatorname{sgn}\left(v_{r\infty}\frac{dv_f}{dx}\right)\boldsymbol{e}_x\end{aligned} \tag{12-82}$$

where C_{LW} is the coefficient of the lift force caused by slanted wake. Here, we assume that the lift force caused by slanted wake pushes the particle towards the negative x direction for positive relative velocity. The coefficient was determined based on the data of Tomiyama et al. (2002) taken under the conditions of $-5.5 \le \log_{10} M \le -2.8$, $1.39 \le Eo \le 5.74$ and $0 \le \left|dv_f/dx\right| \le 8.3\ s^{-1}$, where M and Eo are the Morton number and the Eötvös number, respectively, as defined by

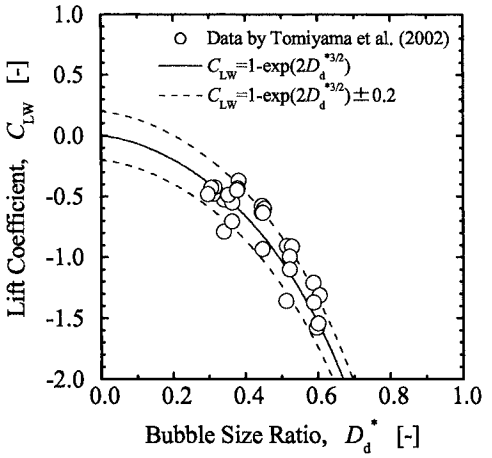

Figure 12-15. Dependence of lift coefficient on bubble size

$$M \equiv \frac{g\left(\rho_f - \rho_g\right)\mu_f^4}{\rho_f^2 \sigma^3} \tag{12-83}$$

$$Eo \equiv \frac{g\left(\rho_f - \rho_g\right)d_b^2}{\sigma}. \tag{12-84}$$

Then, as shown in Fig.12-15, the following correlation of the lift coefficient is proposed based on the data of Tomiyama et al. (2002) as

$$C_{LW} = 1 - \exp\left(2D_d^{*3/2}\right) \tag{12-85}$$

where D_d^* is the ratio of the bubble diameter to the bubble diameter at the distorted bubble limit as

$$D_d^* \equiv \frac{d_b}{4\sqrt{\dfrac{\sigma}{g\Delta\rho}}} = \frac{Eo^{1/2}}{4}. \tag{12-86}$$

We may extend the applicability of Eq.(12-82) in a single particle system to a multiparticle system by replacing $N_{\mathrm{Re}\infty}$ and $G_{s\infty}$ in Eq.(12-82) with N_{Re} and G_s, where the Reynolds number of a multiparticle system, N_{Re}, is defined by Eq.(12-39) and the non-dimensional velocity gradient, G_s, is defined by

$$G_s \equiv \left| \frac{r_d}{v_r} \frac{dv_f}{dx} \right|. \tag{12-87}$$

Thus, the net transverse lift force in multiparticle system, $\boldsymbol{M}_d^L$, is approximated as

$$\begin{aligned} \boldsymbol{M}_d^L &= \frac{\alpha_g}{B_d} \boldsymbol{F}_d^{LT} = -f(G_s, N_{\mathrm{Re}}) \frac{3\alpha_g \rho_f v_r^2}{8 r_d} \mathrm{sgn}\left(v_r \frac{dv_f}{dx} \right) \boldsymbol{e}_x \\ &- C_{LW} f(G_s, N_{\mathrm{Re}}) \frac{3\alpha_g \rho_f v_r^2}{8 r_d} \mathrm{sgn}\left(v_r \frac{dv_f}{dx} \right) \boldsymbol{e}_x . \end{aligned} \tag{12-88}$$

A reasonable agreement between the lift force calculated by Eq.(12-88) with Eq.(12-85) and air-water bubbly flow data (Wang et al., 1987) was obtained, which implies the lift force model, Eq.(12-88) with Eq.(12-85), to be promising to predict the net transverse lift force in multiparticle bubbly flow. Further efforts to examine the applicability of Eq.(12-88) with Eq.(12-85) to a multiparticle system should be made in a future study. As described above, the lift force is still poorly understood, and further experimental and numerical efforts are needed to understand the lift force (Sridhar and Katz, 1995; Ervin and Tryggvason, 1997; Loth et al., 1997).

1.3.2 Wall-lift (wall-lubrication) force

The wall-lift force $\boldsymbol{M}_d^W$ has been introduced and it is explained due to the velocity distribution change around particles near a wall (Antal et al., 1991). This force was used to predict the observed void profiles for cocurrent laminar upward and downward flows. This wall-lift force analogous to a lubrication force acts on a bubble near a wall and prevents the bubbles from touching the wall.

Consider the drainage of the liquid around a bubble moving in the vicinity of a wall. The no-slip condition at the wall should slow the drainage rate between the bubble and the wall, whereas the drainage rate should be increased on the opposite side. Thus, the asymmetrical drainage of the liquid around the bubble in the vicinity of the wall may be quite different

from the symmetrical drainage of the liquid around the bubble in infinite liquid. As a consequence, the bubble experiences a hydrodynamic force, namely wall-lift force, which tends to move the bubble away from the wall. Antal et al. (1991) investigated the wall-lift force acting on a spherical bubble moving in a laminar flow analytically and numerically, and proposed the following functional form

$$\boldsymbol{M}_d^W = \frac{\alpha_g \rho_f \left|\boldsymbol{v}_{\parallel}\right|^2}{r_d}\left[C_{W1} + C_{W2}\left(\frac{r_d}{d_{bw}}\right)\right]\boldsymbol{n}_W \tag{12-89}$$

where $\boldsymbol{v}_{\parallel} = \left(\boldsymbol{v}_g - \boldsymbol{v}_f\right) - \left[\boldsymbol{n}_W \cdot \left(\boldsymbol{v}_g - \boldsymbol{v}_f\right)\right]\boldsymbol{n}_W$, $C_{W1} = -0.104 - 0.06 v_r$ and $C_{W2} = 0.147$. Here, d_{bw} and $\boldsymbol{n}_W$ are the distance between the bubble and the wall, and the unit outward normal vector on the surface of the wall, respectively. Equation (12-89) indicates that the direction of the wall-lift force is reversed at $y_0 = r_d/(0.707 + 0.408 v_r)$, and does not take into account the effect of the bubble deformation near the wall. Further experimental and analytical works should be required to establish the wall-lift force.

1.3.3 Turbulent dispersion force

The turbulent dispersion force $\boldsymbol{M}_d^T$ is due to the bubble motion produced by the turbulent energy of the liquid phase (Lahey et al., 1993). This force was introduced to compensate for the fact that the averaged two-phase continuity equations do not allow for a phasic diffusion effect. The turbulence dispersion force is driven by the void fraction gradient, and tends to flatten the void fraction distribution. On the analogy of the molecular dispersion force, the turbulent dispersion force is expressed by (Lahey et al., 1993)

$$\boldsymbol{M}_d^T = -C_T \rho_f k_f \nabla \alpha_g \tag{12-90}$$

where $C_T = 0.1$ and k_f is the total turbulent kinetic energy of the liquid phase. The applicable flow range of Eq.(12-90) is not clearly given.

1.4 Turbulence in multiparticle system

In a single-phase flow analysis, turbulence structure has been studied extensively, and several turbulence models have been proposed. The turbulence model is commonly classified into zero-equation model, one-

equation model, two-equation model, and stress equation model. The large eddy simulation and direct numerical simulation of the Navier-Stokes equation are also possible. However, in a two-phase flow analysis, limited studies have been performed for turbulence modeling due to the complex nature of the two-phase flow turbulence. In what follows, some preliminary turbulence models in bubbly flow regime are explained briefly. In the models, the turbulent kinetic energy of gas phases is commonly neglected due to the large density difference between gas and liquid phases. To emphasize the time-average, the overbar is applied to a symbol. This subject is also reviewed in Akiyama and Aritomi (2002).

A. Zero-equation Model

The zero-equation turbulence model is commonly expressed as a model with no differential equation to determine the Reynolds stress. In what follows, a model proposed by Sato et al. (1981) will be explained briefly as an example of the zero-equation turbulence model.

Consider two-dimensional fully-developed bubbly flows such as a flow in a vertical pipe or between two parallel flat walls. The y - and z -axes are, respectively, normal and parallel to the main flow direction. This model assumes that (i) only liquid phase contributes to the momentum transfer, and (ii) there are two kinds of turbulences in the liquid phase independent of and dependent on bubble agitation. Then, the velocities in the y - and z - directions, $v_{f,y}$ and $v_{f,z}$ are expressed as

$$v_{f,y} = v'_{f,y} + v''_{f,y} \tag{12-91}$$

$$v_{f,z} = \overline{v_{f,z}} + v'_{f,z} + v''_{f,z} \tag{12-92}$$

where v'_f and v''_f are the liquid velocity fluctuations independent of and dependent on bubble agitation, respectively. $\overline{v_{f,z}}$ is the time-averaged liquid velocity in the z -direction. The turbulent stress for liquid phase, τ_f^T, can be expressed as

$$\tau_f^T = -\rho_f \overline{v'_{f,y} v'_{f,z}} - \rho_f \overline{v''_{f,y} v''_{f,z}} \tag{12-93}$$

where y is the normal-directional distance measured from the channel wall. Here, the eddy diffusivities ε' and ε'' are defined by

$$-\overline{v'_{f,y}v'_{f,z}} = \varepsilon' \frac{\partial \overline{v_{f,z}}}{\partial y} \text{ and } -\overline{v''_{f,y}v''_{f,z}} = \varepsilon'' \frac{\partial \overline{v_{f,z}}}{\partial y}. \tag{12-94}$$

Then, the turbulent stress, τ_f^T, is expressed as

$$\tau_f^T = \rho_f \left(\varepsilon' + \varepsilon''\right) \frac{\partial \overline{v_{f,z}}}{\partial y}. \tag{12-95}$$

Thus, the turbulent stress distribution can be calculated provided ε' and ε'' are given.

For fully developed turbulent bubbly flow, the eddy diffusivity independent of bubble agitation, ε', may be determined empirically based on the Prandtl's mixing length theory and the damping factor in the region close to the smooth wall as

$$\begin{aligned} \varepsilon' = 0.4 &\left\{1 - \exp\left(-\frac{y^+}{16}\right)\right\}^2 \\ &\times \left\{1 - \frac{11}{6}\left(\frac{y^+}{R^+}\right) + \frac{4}{3}\left(\frac{y^+}{R^+}\right)^2 - \frac{1}{3}\left(\frac{y^+}{R^+}\right)^3\right\} \nu_f y^+. \end{aligned} \tag{12-96}$$

Here, $y^+ \equiv y v_f^* / \nu_f$ and $R^+ \equiv R v_f^* / \nu_f$ where v_f^* and R are, respectively, the friction velocity defined by $\sqrt{\tau_w / \rho_f}$ and the radius of a pipe or the half width of a channel with parallel flat walls. The eddy diffusivity that is dependent on bubble agitation, ε'', may be determined empirically based on the virtual kinematic viscosity of a free turbulent flow (such as a wake behind a solid body) and the damping factor in the region close to the smooth wall as

$$\varepsilon'' = 1.2\left\{1 - \exp\left(-\frac{y^+}{16}\right)\right\}^2 \alpha_g \left(\frac{d_B}{2}\right) v_{r\infty} \tag{12-97}$$

where d_B and $v_{r\infty}$ are the mean diameter of the bubbles given by Eq.(12-98) and the terminal velocity in the still liquid, respectively.

$$d_B = \begin{cases} 0 & 0\ \mu\text{m} < y < 20\ \mu\text{m} \\ 4y\left(\widehat{d_B} - y\right)/\widehat{d_B} & 20\ \mu\text{m} \le y \le \widehat{d_B}/2 \\ \widehat{d_B} & \widehat{d_B}/2 < y < R \end{cases} \tag{12-98}$$

where $\widehat{d_B}$ is the cross-sectional mean diameter of the bubbles. The turbulent stress is computed from the above equations and boundary conditions.

B. One-equation Model

The one-equation turbulence model is commonly expressed as a model with only one differential equation of turbulent kinetic energy conservation and constitutive equations for mixing length and other turbulent source terms. In what follows, a model proposed by Kataoka and Serizawa (1995) will be explained briefly as an example of the one-equation turbulence model.

Consider steady, fully developed adiabatic bubbly flows in a round tube. The y - and z-axes are, respectively, normal and parallel to the main flow direction. The turbulent stress, τ_f^T, is expressed in terms of the mixing length of two-phase flow, l_{TP}, and the turbulent velocity, v_t, as

$$\tau_f^T = \rho_f l_{TP} v_t \frac{d\overline{v_{f,z}}}{dy} \tag{12-99}$$

$$v_t \equiv \sqrt{\frac{\overline{\boldsymbol{v}_f' \cdot \boldsymbol{v}_f'}}{3}} \tag{12-100}$$

where $\boldsymbol{v}_f'$ is the liquid velocity fluctuation vector. Thus, the turbulent stress distribution can be calculated provided l_{TP} and v_t are given.

The mixing length of two-phase flow is assumed to be expressed by the linear superposition of the mixing length of the shear-induced turbulence in single-phase liquid flow, l_{SP}, and the mixing length due to the bubble-induced turbulence, l_B, as

$$l_{TP} = l_{SP} + l_B. \tag{12-101}$$

The mixing length of the shear-induced turbulence in single-phase liquid flow is given by

$$l_{SP} = 0.4y\left\{1 - \exp\left(-\frac{yv_f^*}{26\nu_f}\right)\right\}. \tag{12-102}$$

The mixing length of the bubble-induced turbulence is given based on the mechanistic model in which the same volume of liquid is exchanged accompanying the bubble turbulent motion through the control surface as

$$l_B = \begin{cases} \dfrac{1}{3}d_B\alpha_g & \dfrac{3}{2}d_B \le y \le R \\ \dfrac{1}{6}\left\{d_B + \left(y - 0.5d_B\right)\alpha_g\right\} & d_B \le y \le \dfrac{3}{2}d_B \\ \dfrac{1}{6}\left\{d_B + \dfrac{4/3 - \left(y/d_B\right)}{2 - \left(4/3\right)\left(y/d_B\right)}\right\}\alpha_g & 0 \le y \le d_B \end{cases} \tag{12-103}$$

where d_B is the bubble diameter.

The turbulence velocity, v_t, is calculated from the equation of the turbulent kinetic energy for liquid phase given by

$$\begin{aligned} &\frac{1}{R-y}\frac{\partial}{\partial y}\left\{(R-y)\left(1-\alpha_g\right)\left(\frac{\nu_f}{2} + \beta_2\sqrt{k}l_{TP}\right)\frac{\partial k}{\partial y}\right\} \\ &+\beta_1\sqrt{k}l_{TP}\left(1-\alpha_g\right)\left(\frac{\partial\overline{v_{f,z}}}{\partial y}\right)^2 - \gamma_1\left(1-\alpha_g\right)\frac{\left(\sqrt{k}\right)^3}{l_{TP}} \\ &-K_2\alpha_g\frac{\left(\sqrt{k}\right)^3}{d_B} + K_1\frac{3}{4d_B}\alpha_g C_D v_{r\infty}^3\left\{1 - \exp\left(-\frac{yv_f^*}{26\nu_f}\right)\right\} \\ &-\nu_f\left(\frac{\partial\sqrt{k}}{\partial y}\right)^2 = 0 \end{aligned} \tag{12-104}$$

where k is the turbulent kinetic energy of liquid phase given by $k = \overline{\boldsymbol{v}_f' \cdot \boldsymbol{v}_f'}/2$. $\beta_1 (= 0.56)$, $\beta_2 (= 0.38)$, $\gamma_1 = 0.18$, $K_1 (= 0.075)$, and $K_2 (= 1.0)$ are coefficients. In this model, the turbulent velocity is determined by Eq.(12-100) with the assumption of equilateral turbulence as

$$v_t = \sqrt{\frac{2k}{3}}. \tag{12-105}$$

The significance of the various terms in the equation is as follows. The first, second, and third terms on the right-hand side represents the turbulence diffusion, turbulence generation due to shear, and the turbulence dissipation, respectively. The fourth and fifth terms represent the turbulence absorption due to small scale of interface and the turbulence generation due to bubble relative motion, respectively. The last term represents the compensation of numerical error very near to the wall. The turbulent stress is computed from the above equations and boundary conditions.

C. Two-equation Model

The two-equation turbulence model is commonly expressed as a model with two differential equations to determine the Reynolds stress. In what follows, k-ε model proposed by Lopez de Bertodano et al. (1994) will be explained briefly as an example of the two-equation turbulence model.

Consider steady, fully developed adiabatic dilute bubbly flows. The turbulent stress tensor, $\mathbb{T}_f^T$, is assumed to be expressed by the linear superposition of the shear-induced (SI) turbulent stress tensor, $\mathbb{T}_f^{SI}$, and the bubble-induced (BI) turbulent tensor, $\mathbb{T}_f^{BI}$, as

$$\mathbb{T}_f^T = \mathbb{T}_f^{SI} + \mathbb{T}_f^{BI}. \tag{12-106}$$

The shear-induced turbulent stress is computed by

$$\mathbb{T}_f^{SI} = \rho_f \nu_t \left\{ \nabla \overline{\boldsymbol{v}_f} + \left(\nabla \overline{\boldsymbol{v}_f} \right)^+ \right\} - \frac{2}{3} \mathbb{A} \rho_f k^{SI} \tag{12-107}$$

where ν_t, $\mathbb{A}$ and k^{SI} are the turbulent kinematic viscosity, the turbulence anisotropy tensor and the turbulent kinetic energy due to the shear-induced turbulence, respectively. For the isotropic turbulence, $\mathbb{A} = \mathbb{I}$.

The bubble-induced turbulence is computed by

$$\mathbb{T}_f^{BI} = -\alpha_g \rho_f \left(\frac{1}{20} \overline{\boldsymbol{v}_r} \overline{\boldsymbol{v}_r} + \frac{3}{20} \left| \overline{\boldsymbol{v}_r} \right|^2 \mathbb{I} \right) \tag{12-108}$$

$$= -\alpha_g \rho_f \frac{1}{2} C_{vm} \left|\overline{\boldsymbol{v}_r}\right|^2 \begin{pmatrix} 4/5 & 0 & 0 \\ 0 & 3/5 & 0 \\ 0 & 0 & 3/5 \end{pmatrix}$$

where C_{vm} is the virtual volume coefficient, and the value for potential flow around a sphere is 1/2. The value of 2.0 and 1.2 are recommended for the low and high void fraction cases, respectively. The turbulent kinetic energy due to the bubble-induced turbulence, k^{BI}, can be obtained as

$$k^{BI} = \alpha_g \frac{1}{2} C_{vm} \left|\overline{\boldsymbol{v}_r}\right|^2 . \tag{12-109}$$

Then, substituting Eqs.(12-108) and (12-107) into Eq.(12-106), yields

$$\overline{\mathbb{T}}_f^T = \rho_f \nu_t \left\{ \nabla \overline{\boldsymbol{v}_f} + \left(\nabla \overline{\boldsymbol{v}_f} \right)^+ \right\} - \frac{2}{3} \mathbb{A} \rho_f k^{SI} - \alpha_g k^{BI} \begin{pmatrix} 4/5 & 0 & 0 \\ 0 & 3/5 & 0 \\ 0 & 0 & 3/5 \end{pmatrix}. \tag{12-110}$$

Thus, the shear stress distribution can be calculated provided ν_t and k^{SI} are given.

The turbulent kinematic viscosity is assumed to be expressed by the linear superposition of the turbulent kinematic viscosities due to the shear-induced turbulence, ν_t^{SI}, and the bubble-induced turbulence, ν_t^{BI} as

$$\nu_t = \nu_t^{SI} + \nu_t^{BI} . \tag{12-111}$$

The turbulent kinematic viscosities due to the shear-induced turbulence and the bubble-induced turbulence are given as Eqs.(12-112) and (12-113), respectively.

$$\nu_t^{SI} = 0.09 \frac{{k^{SI}}^2}{\varepsilon^{SI}} \tag{12-112}$$

where ε_{SI} is the dissipation of the shear-induced turbulence.

$$\nu_t^{BI} = 1.2\frac{d_B}{2}\alpha_g\left|\overline{\boldsymbol{v}_r}\right| \tag{12-113}$$

The turbulent kinetic energy and dissipation due to the shear-induced turbulence can be computed by the shear-induced turbulence kinetic energy transport equation given by Eq.(12-114) and the shear-induced turbulence dissipation rate transport equation given by Eq.(12-116).

$$\alpha_f\frac{Dk^{SI}}{Dt} = \nabla\cdot\left(\frac{\alpha_f\nu_t}{\sigma_k}\nabla k^{SI}\right) + \alpha_f\left(P^{SI} - \varepsilon^{SI}\right) \tag{12-114}$$

where $\sigma_k\,(=1.0)$ is a constant and P^{SI} is the production of the shear-induced turbulence given by

$$P^{SI} \equiv \nu_t\left\{\nabla\overline{\boldsymbol{v}_f} + \left(\nabla\overline{\boldsymbol{v}_f}\right)^+\right\} : \nabla\overline{\boldsymbol{v}_f} \tag{12-115}$$

$$\alpha_f\frac{D\varepsilon^{SI}}{Dt} = \nabla\cdot\left(\alpha_f\frac{\nu_t}{\sigma_\varepsilon}\nabla\varepsilon^{SI}\right) + \frac{\alpha_f\varepsilon^{SI}}{k^{SI}}\left(C_{\varepsilon 1}P_{SI} - C_{\varepsilon 2}\varepsilon^{SI}\right) \tag{12-116}$$

where $\sigma_\varepsilon\,(=1.3)$, $C_{\varepsilon 1}\,(=1.44)$, and $C_{\varepsilon 2}\,(=1.92)$ are constants. The turbulent stress is computed from the above equations and boundary conditions.